Royal Netherlands Meteorological Institute
Ministry of Infrastructure and the Environment

The EUMETSAT Network of Satellite Application Facilities

OSI SAF
Ocean and Sea Ice

EUMETSAT

Ocean and Sea Ice SAF

CMOD7

SAF/OSI/CDOP2/KNMI/TEC/RP/237

23 November 2015

Jeroen Verspeek
Ad Stoffelen

Royal Netherlands Meteorological Institute (KNMI)
De Bilt, the Netherlands

Summary

A new GMF is being developed for C-band scatterometers. CMOD6 is used for ERS and ASCAT and is valid for their combined incidence angle range. For low winds there is a clear mismatch between CMOD6 and the measurements. C2013 is valid for ASCAT only and performs especially well for low winds. The new GMF (CMOD7) uses both CMOD6 and C2013 and shows improvements in the retrieved wind distribution compared to CMOD6 and C2013, while retaining its validity for both ERS and ASCAT.

Contents

1 Introduction

Within the framework of the EUMETSAT Ocean & Sea Ice (OSI) Satellite Application Facility (SAF) and Numerical Weather Prediction (NWP) SAF, KNMI is continuously developing the wind processor for the ERS and ASCAT C-band scatterometers.

The ASCAT wind processor (AWDP) wind inversion process uses a forward model or Geophysical Model Function (GMF), which translates, for a given measurement geometry, wind speed and direction to a radar backscatter value. The empirical C-band GMFs are based on the European Remote-Sensing (ERS) mission scatterometer, called ESCAT [Stoffelen, 2011]. Since ASCAT has a slightly extended incidence angle range, the outer swath ASCAT GMF is based on an extrapolation of the ESCAT data.

CMOD4 and CMOD5 were initially verified with 10m wind. However, 10m winds depend not only on the sea surface roughness as sensed by a scatterometer, but also on the atmospheric stability in the lowest 10m of the atmosphere and on the air mass impact on the ocean surface, hence air mass density. The former effect was taken into account when equivalent-neutral winds were introduced in C-band scatterometry [Portabella and Stoffelen, 2006; Hersbach et al., 2007], called U10N. More recently, not U10N is used to validate scatterometer-retrieved winds, but rather the stress-equivalent 10m wind, called U10S, which takes account of the effect of air mass density [Scirocco team, 2014].

For ASCAT CMOD5N is used operationally in combination with an incidence-angle dependent correction, yielding CMOD6. On top of this an antenna specific and Wind Vector Cell (WVC) dependent correction is applied to correct for small instrumental inconsistencies, see [Verspeek, 2012].

Recently, it was verified [Anderson et al, 2012] that inconsistencies exist between the mid beam and the fore and aft beams of the ERS-1 scatterometer (ESCAT-1) at low backscatter values. Since CMOD5N is based on ESCAT, it also incorporates irregularities at low wind speeds.

Ricciardulli et al. [Ricciardulli 2012; 2014] have developed a new GMF for C-band scatterometers (C2013) from four years of (uncorrected) ASCAT data collocated with SSMI and WindSat data. In this report we exploit the analysis tools developed for ESCAT and ASCAT to measure the performances of CMOD6 and C2013 with the aim to build an improved GMF.

2 A consistent C-band GMF for ERS and ASCAT

The CMOD GMF was originally developed by fitting a parameter function to ERS data. The ASCAT scatterometers on the Metop satellites are very similar to the ERS scatterometers in many respects but have the swaths somewhat further away from the satellite ground track, giving rise to higher incidence angles. When the first ASCAT-A data became available it turned out that the GMF, CMOD5 at that time, was not fit to the higher incidence angles of ASCAT and showed large deviations of up to 1 dB in NWP Ocean Calibration (NOC) residuals.

The NOC residuals were used as correction factors and can be split in antenna dependent corrections, and a correction that only depends on incidence angle. The latter was incorporated in the GMF yielding CMOD5na [Verspeek, 2012].

Recently with the idea of building a consistent climate data record from scatterometer data the need for a GMF that fits both ASCAT and ERS emerged. We have CMOD5n which works well for ERS but was not fit to the higher ASCAT incidence angles, and we have CMOD5na which works well for ASCAT but was not fit to the lower ERS incidence angles.

Originally the NOC residuals from ASCAT were fitted with a 3rd order polynomial yielding CMOD5na. This works fine for the ASCAT incidence angle range but the fit is not valid for the lower ERS incidence angles. Therefore a new fit on the same ASCAT data was performed, a 5th order polynomial with boundary condition $d(\Delta B_0)/d\theta=0$ at $\theta=20^0$ yielding CMOD6. The extra boundary condition forces a more or less flat correction at the lower incidence angles around $\theta=20^0$ making it valid for ERS also.

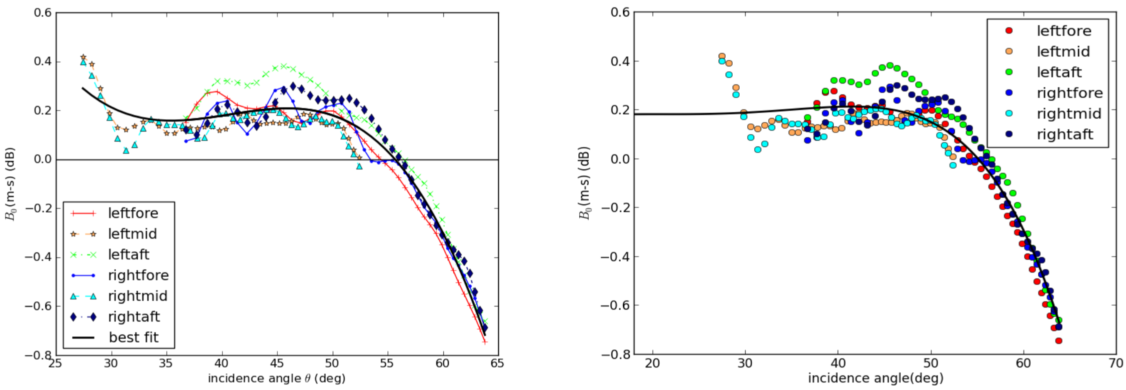

a) b)

Figure 1–NOC residuals from one year of ASCAT data.
a) shows a third order polynomial fit, defining CMOD5na. It is valid only for the shown ASCAT incidence angle range.
b) shows a fifth order polynomial fit with the additional boundary condition that the derivative is zero at a incidence angle of 20^0, defining CMOD6. It is valid for the combined ERS and ASCAT incidence angle range.

In Figure 2 NOC residuals from one year of ERS data is shown for several GMFs. The ECMWF U10 winds are used with a 0.2 m/s correction for comparison with the scatterometer neutral 10 m winds. Figure 2a) and Figure 2b) show the NOC residuals for C2013 and CMOD5na. As can be seen these residuals show large values for the low incidence angles. In Figure 2c) and Figure 2d) the NOC residuals for CMOD5n and CMOD6 are shown. These GMFs are valid for the ERS incidence angle range and have much smaller values for the low incidence angles. As stated before, CMOD5n is not valid for the higher ASCAT incidence angle range, but CMOD6 is valid over the whole combined ERS/ASCAT incidence angle range.

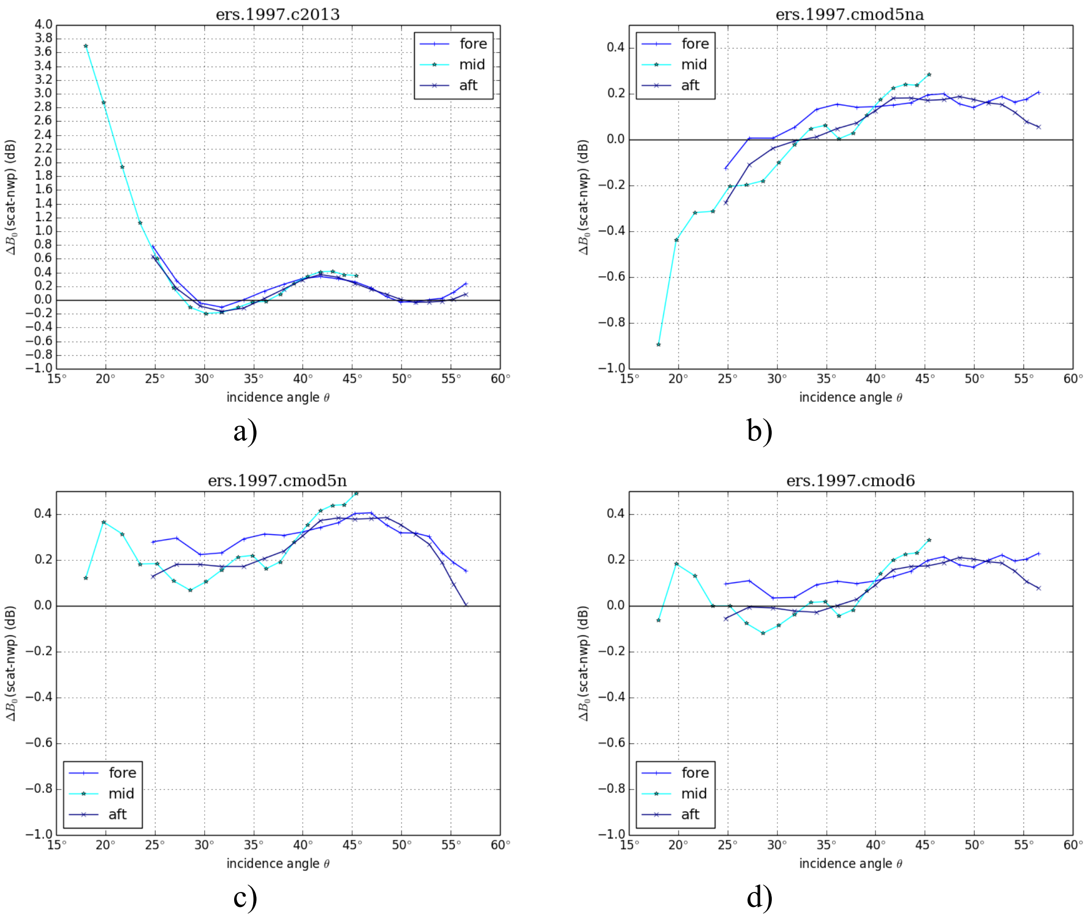

Figure 2 – NOC residuals from one year of ERS data with GMF a) C2013, b) CMOD5na, c) CMOD5n and d) CMOD6.

3 C-band GMF

In Figure 3 and Figure 4 the CMOD6 and C2013 are shown for comparison. Figure 3 shows the backscatter as a function of input wind speed for incidence angles corresponding to the fore and aft antenna WVCs. Figure 4 shows CMOD6 (colors) and C2013 (black) for a fixed WVC in the middle of the swath.

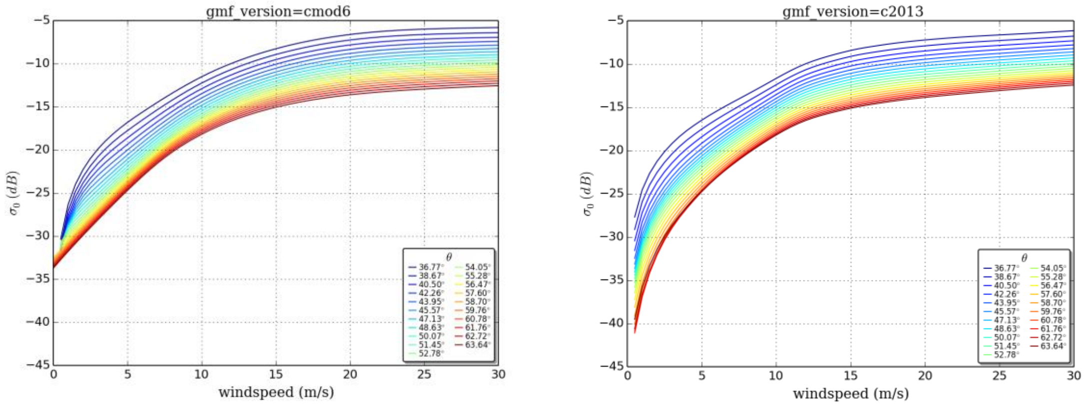

Figure 3 – Comparison between CMOD6 (left) and C2013 GMF (right). Backscatter as a function of wind speed at some fixed incidence angles.

CMOD6 and C2013 are rather close for wind speeds between 5 and 15 m/s, but otherwise differences do occur:

- For low wind speeds CMOD6 converges to a value of about -33 dB for zero speed;
- For wind speeds above 15 m/s CMOD6 shows more dispersion with incidence angle than C2013 and more saturation;
- The upwind-crosswind modulation of C2013 is much smaller than that of CMOD6 for low wind speeds;

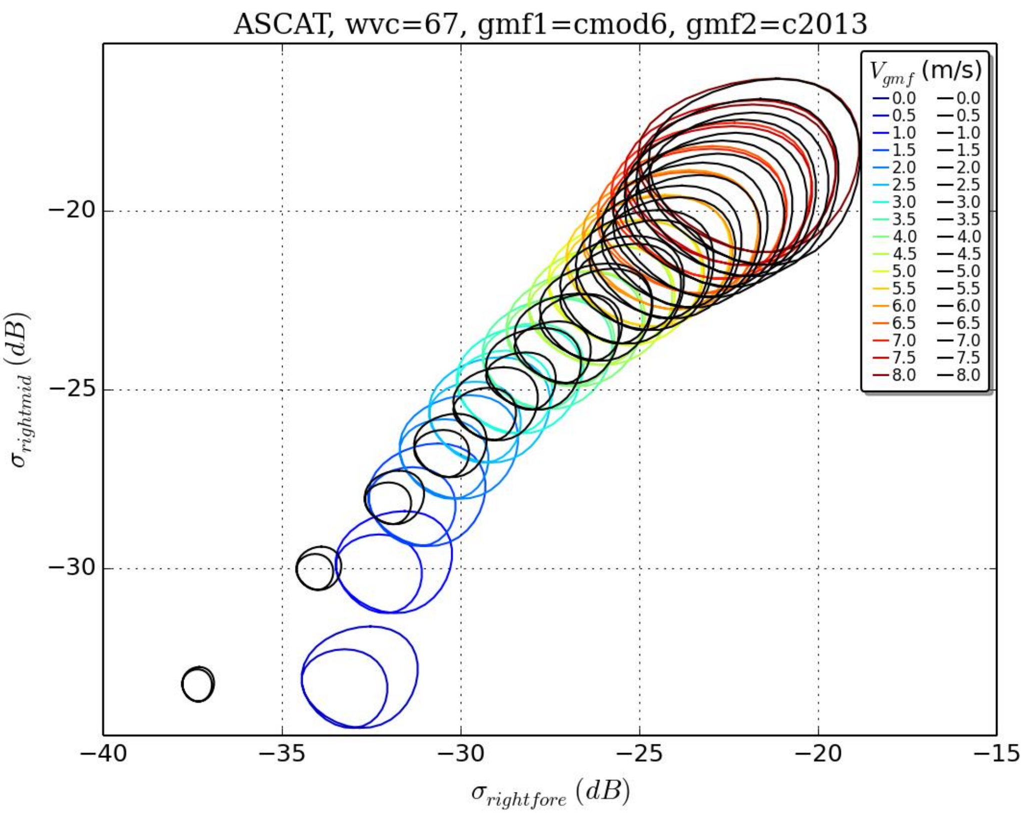

Figure 4 – Comparison between CMOD6 (colors) and C2013 GMF (black) fore versus mid antenna backscatter for given wind speeds up to 8 m/s at WVC 67 (12.5 km WVC spacing).

4 ASCAT measurement space

The radar backscatter triplets can be visualized in the 3-dimensional measurement space where the three axes correspond to the backscatter to each of the respective antennas. For a given WVC, i.e., position across the swath, the measured triplets are distributed around the GMF, which represents a double-folded conical surface. In Figure 5 a visualization of the data and GMF is shown for CMOD6 (blue) and C2013 (red) for WVC 62 (middle of right swath at 12.5 km WVC spacing). The cross section of the GMF with the plane $\sigma_{fore} = \sigma_{aft}$ is shown. The data is from one week reprocessed with CMOD6 . For CMOD6 the mismatch in the tail between data and GMF can be clearly seen. This mismatch is most prominent for WVCs in the middle of the swaths.

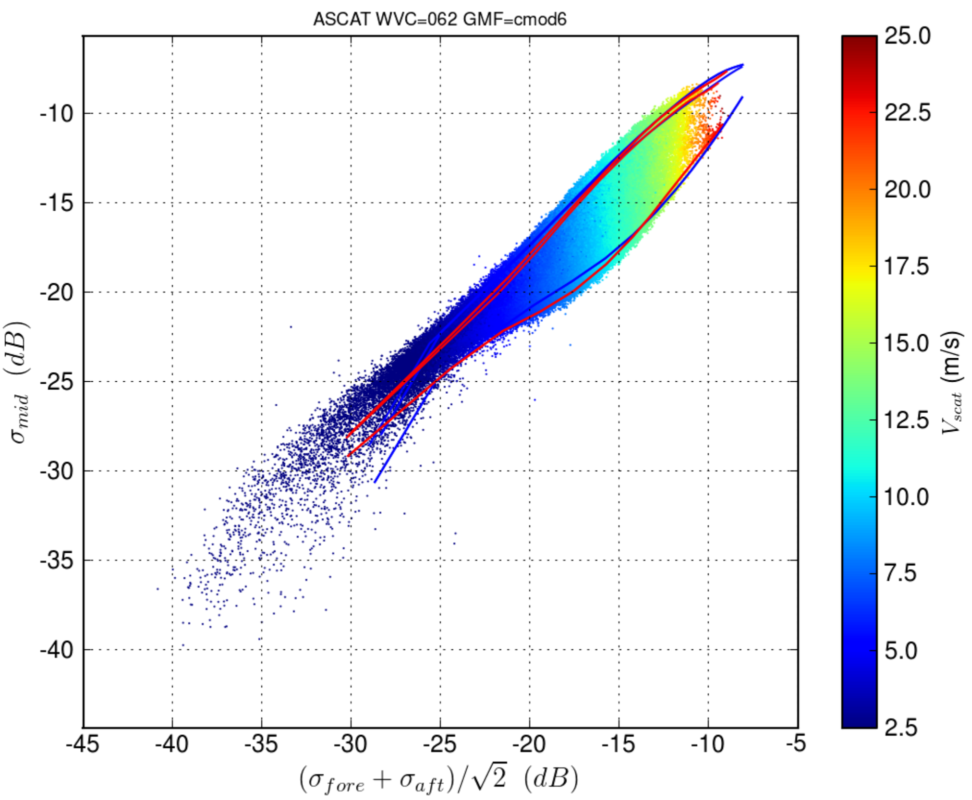

Figure 5 – Visualization of data and GMF in measurement space for CMOD6 (blue) and C2013 (red) for WVC 62 (12.5 km WVC resolution).

In Figure 6 visualizations are shown for CMOD6 (blue) and C2013 (red) in z-coordinate space. z coordinates are obtained by the transformation of linear coordinates where $z = \sigma_0^{0.625}$. The z transformation yields a more circular distribution of measurement points as compared to the same cross section in linear coordinate space (see [Stoffelen and Anderson

1997]). For C2013 the cross section becomes triangular in z coordinates, which may explain the degraded QC at modal and higher winds due to higher rejection rates.

The constant C which defines the cross-section plane corresponds to the B_0 value from CMOD6 at the indicated wind speeds of 0.5, 2.5, 5.0, 8.0, 15,0 and 20.0 m/s. The value of C is different from the value that would be derived from C2013 for the same wind speed due to differences in wind speed labeling between the two GMFs, but does not affect the proximity of the GMF and data points.

Data points that are within a distance of 0.05C from the plane are plotted also. Clearly the C2013 GMF fits the data cloud better for V=0.5 m/s.

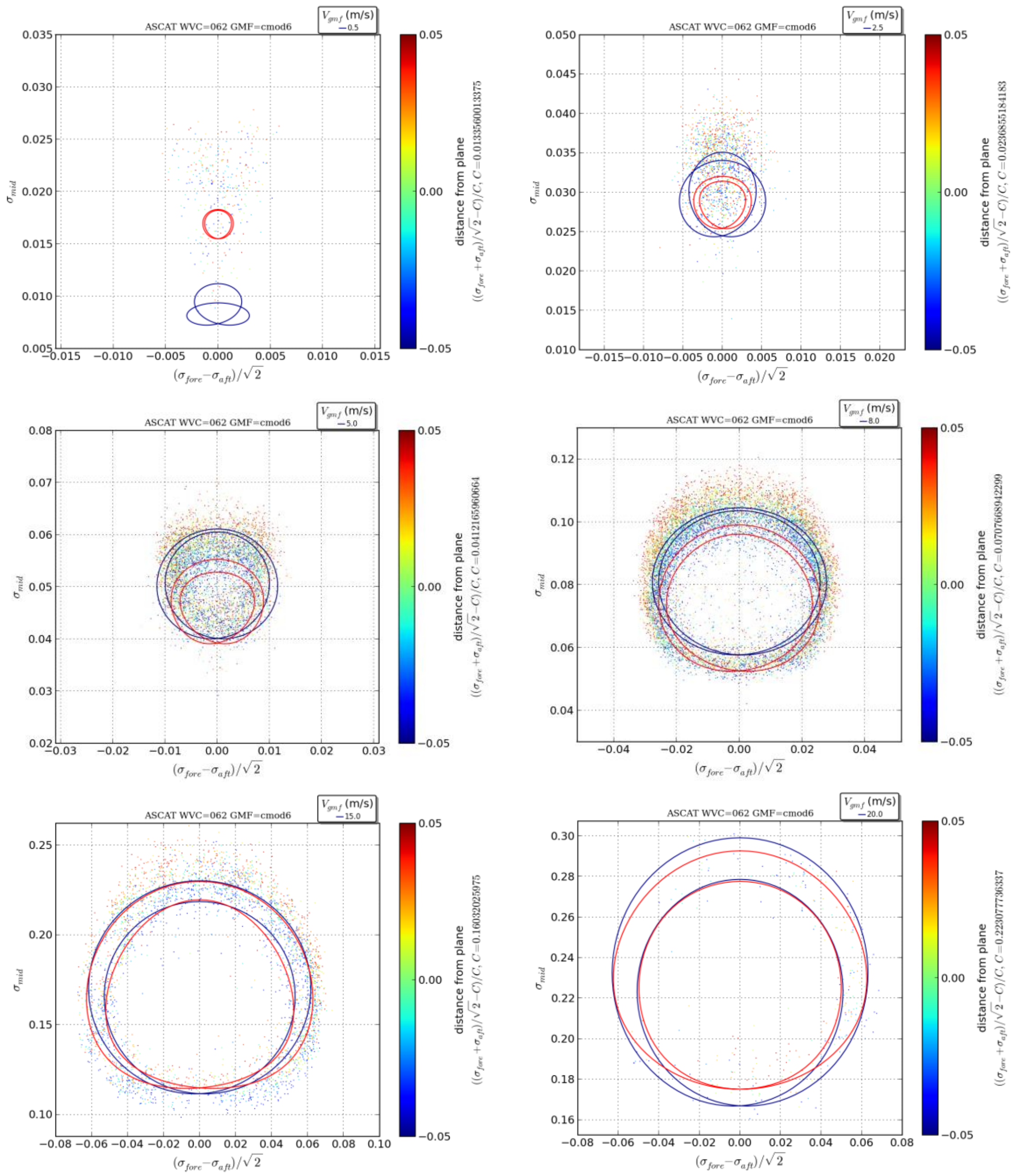

Figure 6 - Visualization of observed data (dots) and GMF in measurement space for CMOD6 (blue) and C2013 (red). The constant C defines the cross-section plane and corresponds to the B_0 value from CMOD6 at the indicated wind speeds of 0.5, 2.5, 5.0, 8.0, 15,0 and 20.0 m/s.

5 Wind, MLE and QC statistics (CMOD6-C2013)

In order to evaluate the GMFs, ASCAT-B data from January 2013 has been reprocessed using the 12.5 km WVC coastal sampling. In Figure 7 the contour plots from the scatterometer wind against the ECMWF wind is shown for CMOD6 (left) and C2013 (right). As can be seen the C2013 winds above 15 m/s are biased high against the ECMWF (and thus against buoy) winds.

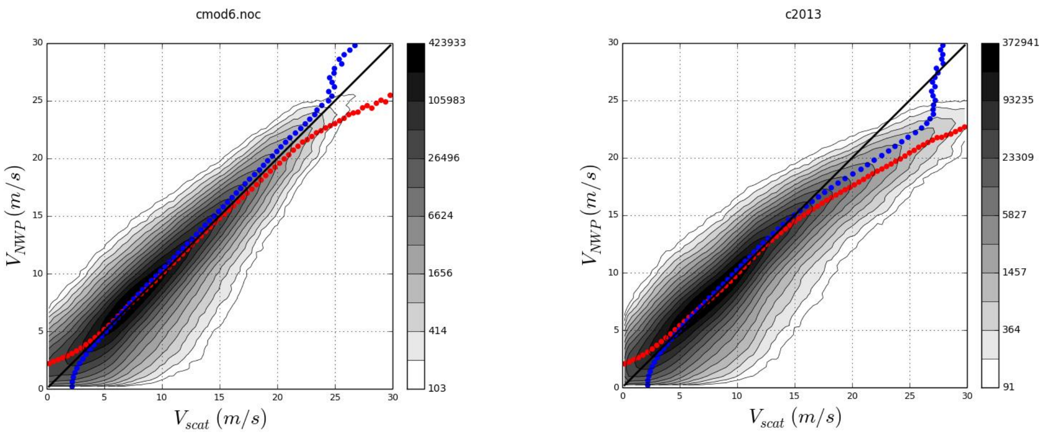

Figure 7 – Scatterometer wind versus ECWMF wind for ASCAT data processed with CMOD6 (left) and C2013 (right).

In Figure 8 the wind direction histograms per wind speed interval are shown for scatterometer winds from CMOD6, C2013 and NWP winds from ECWMF. Both the scatterometer and ECMWF are known to have little wind direction skill for low winds. In the ASCAT wind inversion this leads to an artificial preference for certain wind directions (the across track and along track wind direction), but in ECMWF it leads to a rather uniform wind direction distribution. This shows up in the polar wind direction histograms. However, as can be seen the artifacts are larger for CMOD6 than for C2013.

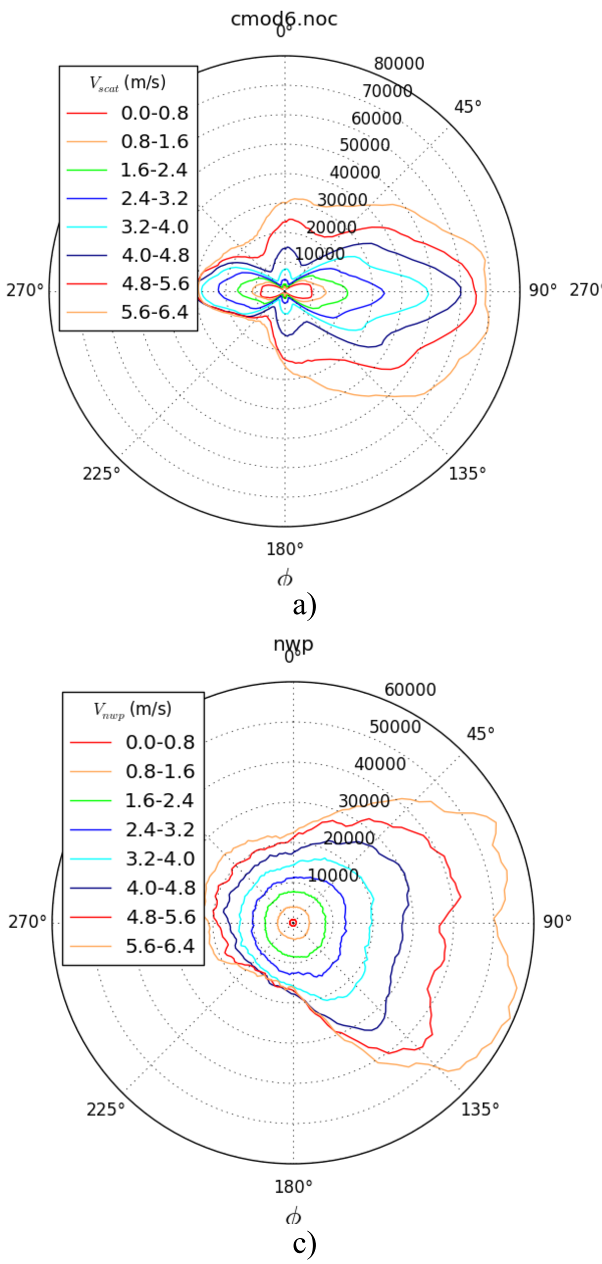

Figure 8 – Wind direction distribution per wind speed interval for winds from a) CMOD6, b) C2013 and c) ECWMF.

The CMOD6 speed and direction artifacts at low speed may be improved with respect to C2013.

In Figure 9 the Maximum Likelihood Estimate (MLE) is shown as a function of scatterometer wind speed (above) and as a function of WVC number (bottom) for retrievals with CMOD6 and C2013. The MLE is a direct measure of the distance from a measured triplet to the cone surface as defined by the GMF. It is normalized such that its expectation value is unity. A positive MLE value corresponds to a triplet positioned inside the cone, a negative MLE value to a triplet outside the cone (actually the MLE sign corresponds to the sign of the curvature of the cone at the point where the triplet is projected on the cone).

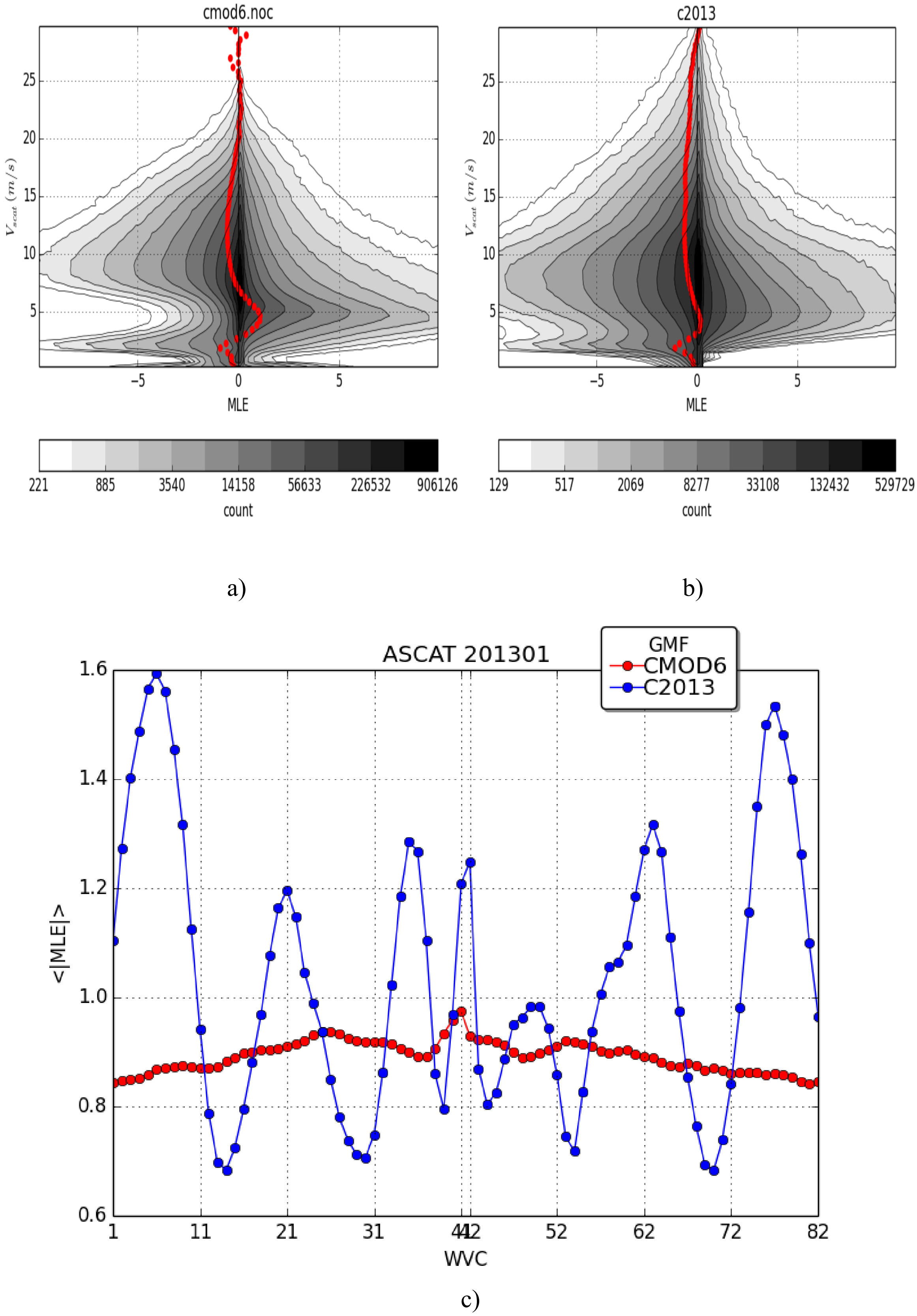

Figure 9 – MLE of selected wind solution as a function of scatterometer wind speed (a and b) and as function of WVC for CMOD6 and C2013.

For high winds the radius of the cone is quite large compared to the standard deviation of the distance to cone of the measured triplets. Thus the distribution of triplets around the cone surface is symmetrical as well as the MLE distribution. For lower winds the radius of the cone becomes smaller and the standard deviation of the distance to cone becomes larger. The probability that the Ambiguity Removal (AR) will select a wrong solution with a wrong sign increases, which gives rise to the asymmetry in the MLE distribution as seen in Figure 9a for CMOD6. In Figure 9b for C2013 the asymmetry is less pronounced which is an indication that AR is performing better due to a better positioning of the GMF cone in measurement space, thus lower MLE and generally better wind retrieval.

The MLE as a function of WVC number in Figure 9c (C2013) shows a wiggly pattern which is not present for CMOD6. Also the average values of the MLE for C2013 are slightly higher than for CMOD6. The wiggly pattern can be observed in ocean calibration results as well. In contrast with C2013, for CMOD6 NOC corrections are applied which cancel out the wiggles [Verspeek, 2012].

During processing, Quality Control (QC) flags can be set depending on various conditions encountered. In Figure 10 several QC flag rates are shown as a function of WVC number for CMOD6 and C2013. For the comparison of the rejection rate the knmi_qc bit and the var_qc bit are of interest. The knmi_qc flag bit is set when wind retrieval fails or is suspect. It incorporates several other flag bits like Kp, inversion and gmf_distance. The var_qc bit is set when the 2d-var ambiguity removal fails or is suspect. The knmi_qc bit and var_qc bit are set mutually exclusive and their sum is monitored as rejection rate in the operational processing. The top figures show overall flag rates and the bottom figures are for NWP winds lower than 6 m/s only.

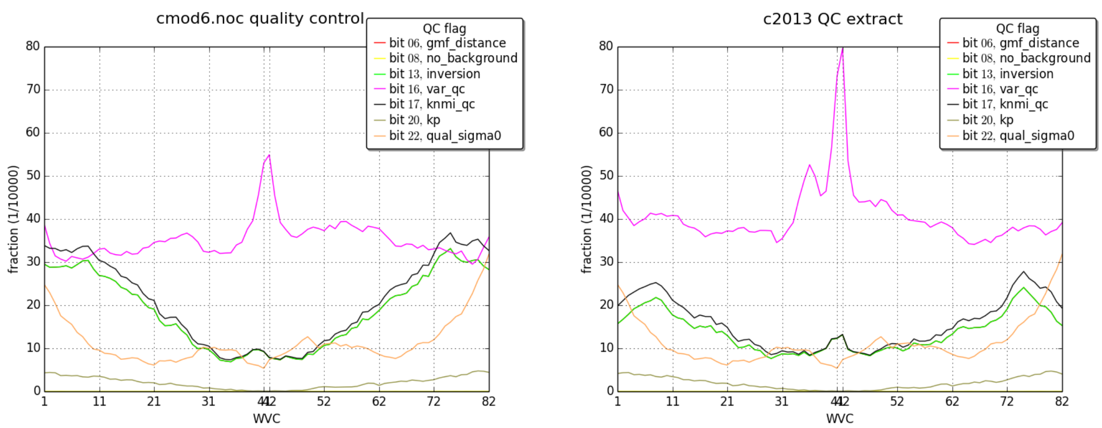

a) b)

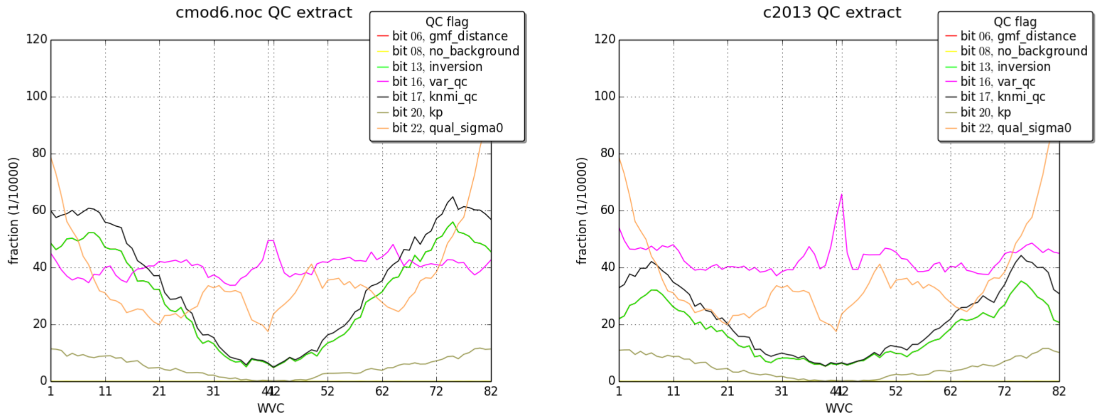

c) d)

Figure 10 – Quality Control rejection rate as a function of WVC number for a) CMOD6 and b) C2013. Figure c) and d) are for NWP winds lower than 6 m/s only.

As can be seen in the top figures the knmi_qc rejection rate is lower for C2013 and the var_qc rejection rate is somewhat higher. For the bottom figures (low winds) the knmi_qc rejection rate is lower and the var_qc rejection rate about the same. Especially at high incidence angles the rejection rate is lower. The table below summarizes the rejection rates. The overall rejection rate is about the same for CMOD6 and C2013 but for low winds C2013 clearly has less rejections and for modal and high winds more. It would be of interest to combine both GMFs, where C2013 is adopted at low winds and CMOD6 at modal and high winds.

Table 1 - Quality Control rejections in 1000s

	Total	knmi_qc	var_qc	rejections	rejection rate
cmod6	52646	110	185	295	0.0056
c2013	52646	83	214	297	0.0056
cmod6 (Vnwp<6m/s)	16227	57	65	123	0.0076
c2013 (Vnwp<6m/s)	16227	36	70	106	0.0065
cmod6 (Vnwp>6m/s)	36419	53	120	173	0.0048
c2013 (Vnwp>6m/s)	36419	47	144	191	0.0053

6 Combined GMF

The CMOD6 and C2013 are combined into a new GMF: CMOD7. It uses an interpolation in the wind speed domain between 2.4 m/s and 7.0 m/s and in the incidence angle domain between 27^{o} and 37^{o}. CMOD7 should have improved low winds compared to CMOD6 but will remain identical to CMOD6 for winds above 7.0 m/s and for incidence angles below 27^{o}.

An independent interpolation is performed in the wind domain from 2.4 to 7.0 m/s for each combination of incidence and azimuth angle . The inverted weight distance is used with a power of 2. In Figure 11 the weight function is shown for several values of the power. The higher the power the sharper the transition around V=4.7 m/s will be. The chosen function gives a smooth transition towards the edges of the interpolation interval. A similar interpolation curve is used in the incidence angle domain.

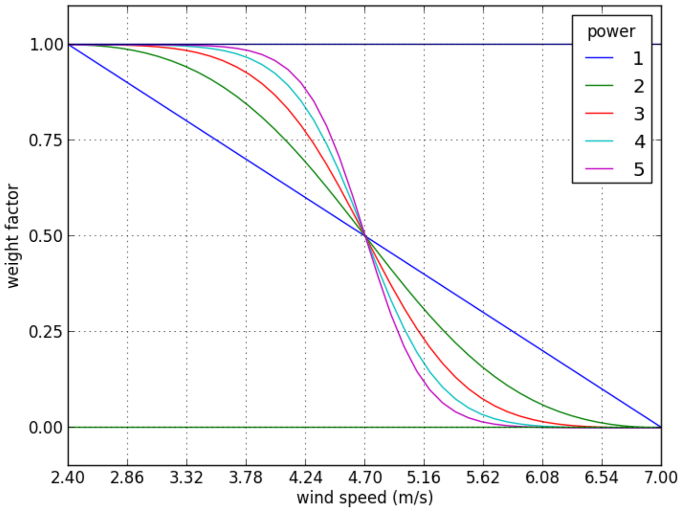

Figure 11 – Weight function for the inverted-weight distance interpolation

In Figure 12 the interpolation regions for CMOD7 are shown in the wind speed-incidence angle domain. The upper bound of the incidence angle interpolation region of 37^{o} is chosen such that only the ASCAT mid beam is affected. The CMOD6 low-wind artefacts are prominent for the high incidence angles, but almost not present for the low incidence angles used in the interpolation region. So CMOD7 will still strongly reduce the low wind artefacts while the incidence angle interpolation extends the validity of CMOD7 to ERS.

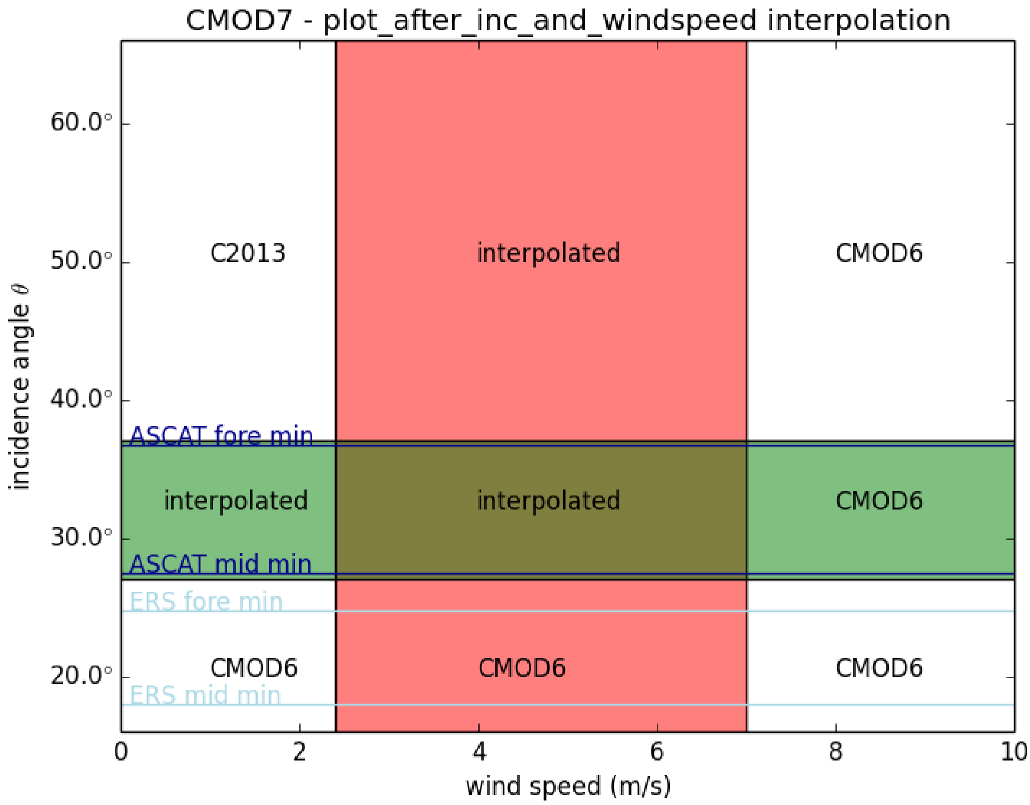

Figure 12 – Interpolation regions for CMOD7.

Figure 13 shows the differences between CMOD6 and CMOD7 for the ERS mid beam incidence angle range. Difference shown up only for the low wind speed/high incidence angle domain.

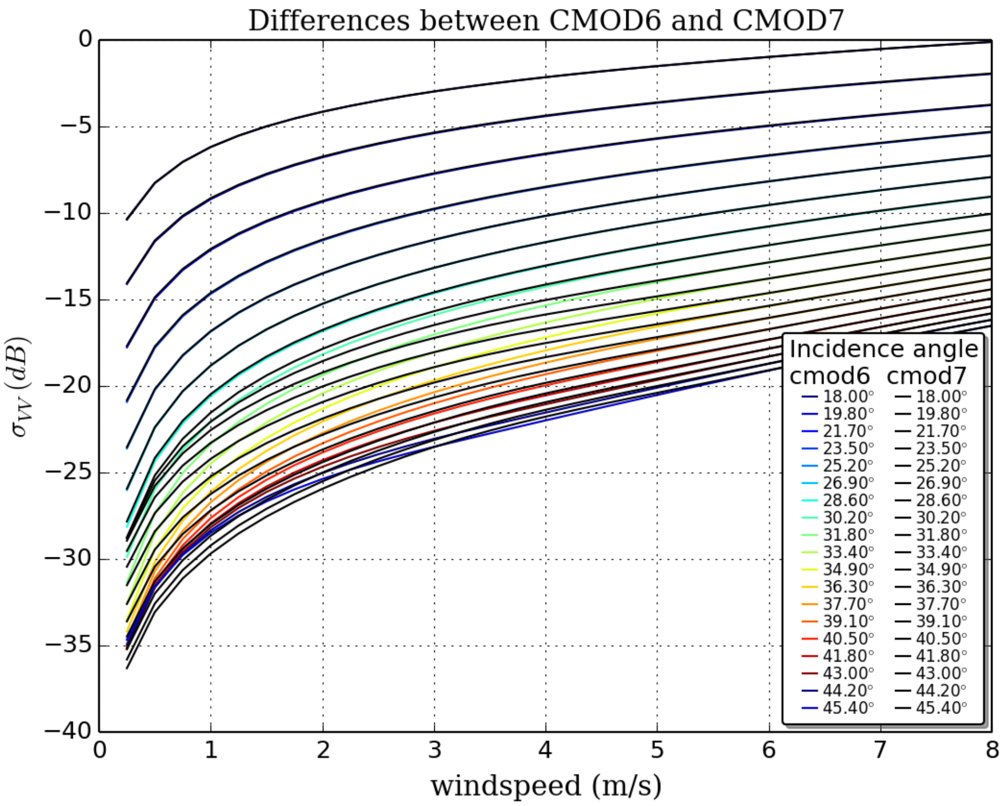

Figure 13 - Differences between CMOD6 (colors) and CMOD7 GMF (black). Backscatter as a function of wind speed at some fixed incidence angles. The incidence angles correspond to the ERS mid beam range.

7 Wind, MLE and QC statistics (CMOD6-CMOD7)

In this section a comparison is made between the wind, MLE and QC statistics of CMOD6 and CMOD7 in analogy with section 5 (CMOD6 and C2013). In Figure 14 the contour plots from the scatterometer wind against the ECMWF wind is shown for CMOD6 (left) and CMOD7 (right). Both contour plots look the same, small differences are present for the low winds only because both GMFs are identical for winds above 7.0 m/s.

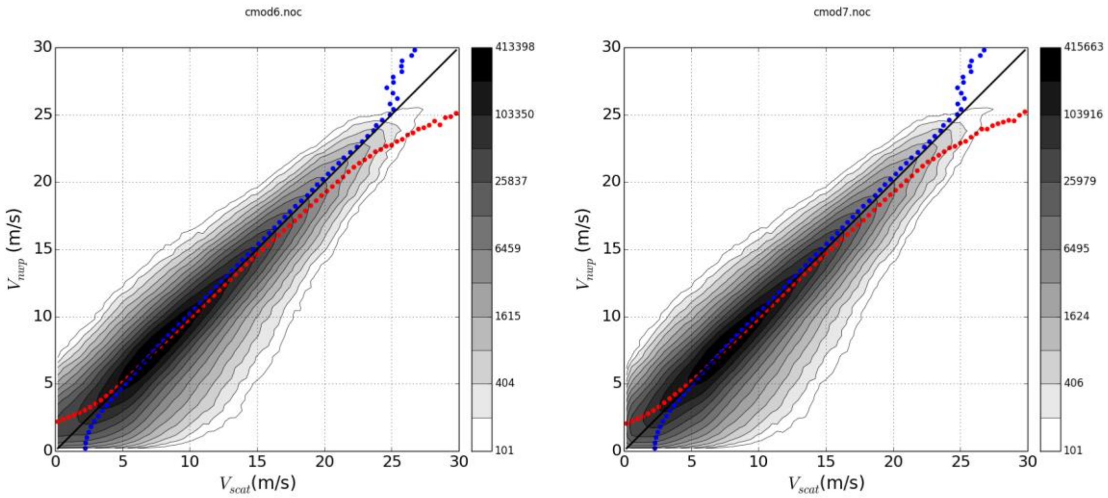

Figure 14 – Scatterometer wind versus ECWMF wind for ASCAT data processed with CMOD6 (left) and CMOD7 (right).

In Figure 15 the scatterometer wind speed, wind direction, and the u and v wind components are shown for ASCAT data processed with CMOD7 (horizontal axis) against CMOD6 (vertical axis). Differences are clear now for the low wind speeds. In the wind direction double peaks are visible that correspond to 2DVAR differences at the across track and along track direction. The scatterometer satellite track direction is somewhat different for ascending and descending tracks which correspond to the closely paired peaks.

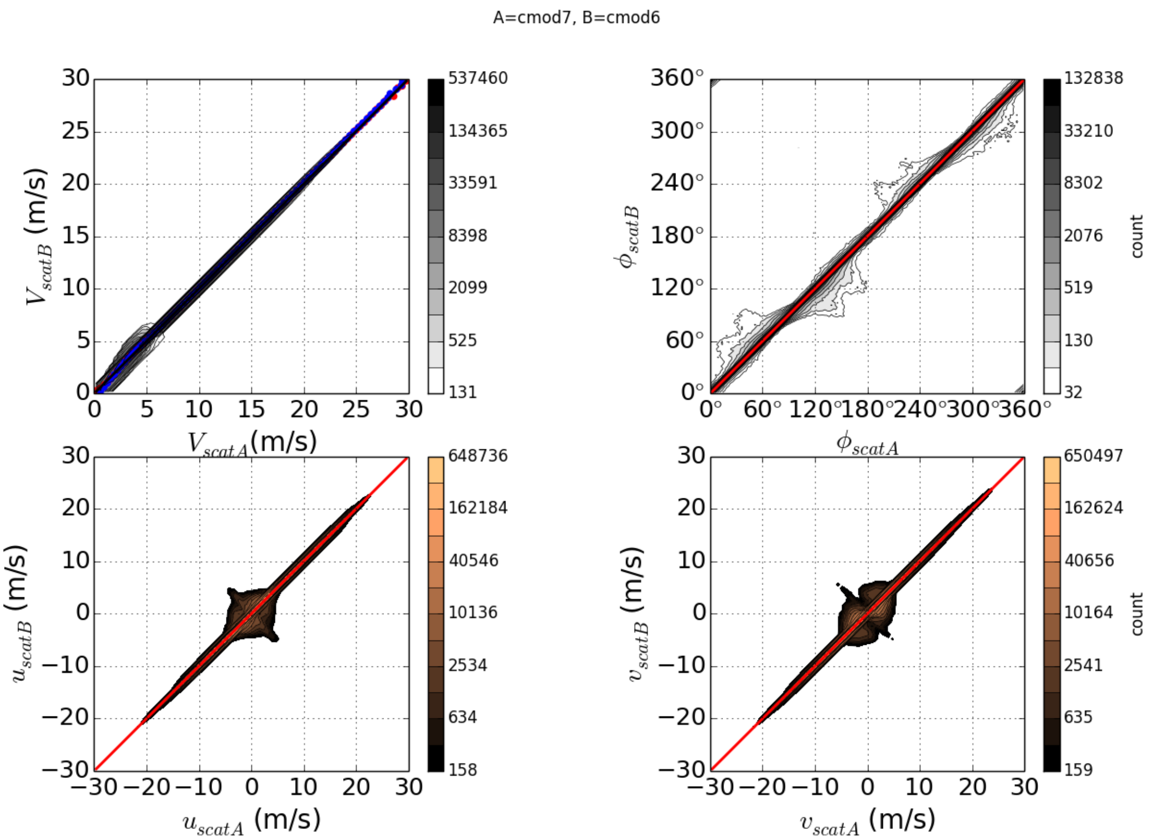

Figure 15 – Scatterometer wind speed (top left), wind direction (top right), u-component (bottom left) and v-component (bottom right) for ASCAT data processed with CMOD7 (horizontal axis *A*) against CMOD6 (vertical axis *B*).

In Figure 16 the wind direction histograms per wind speed interval are shown for scatterometer winds from CMOD6 and CMOD7 winds. As can be seen the wind direction distribution shows less pronounced artifacts for low winds for CMOD7 than for CMOD6.

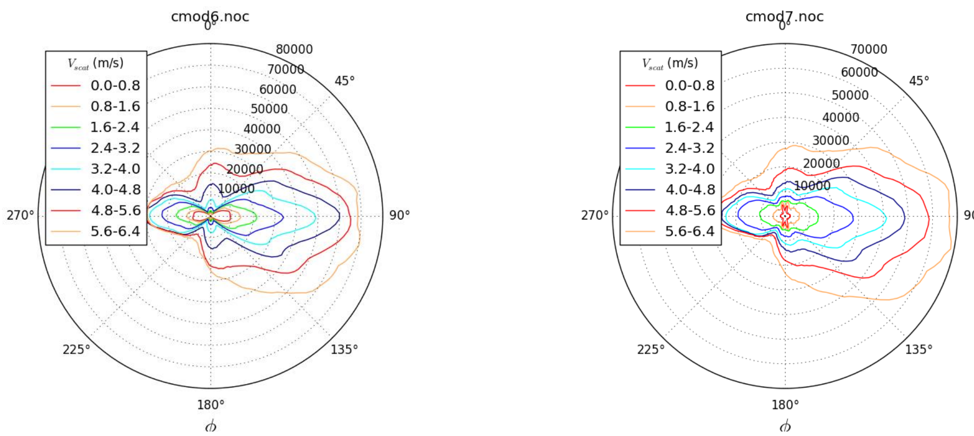

a) b)

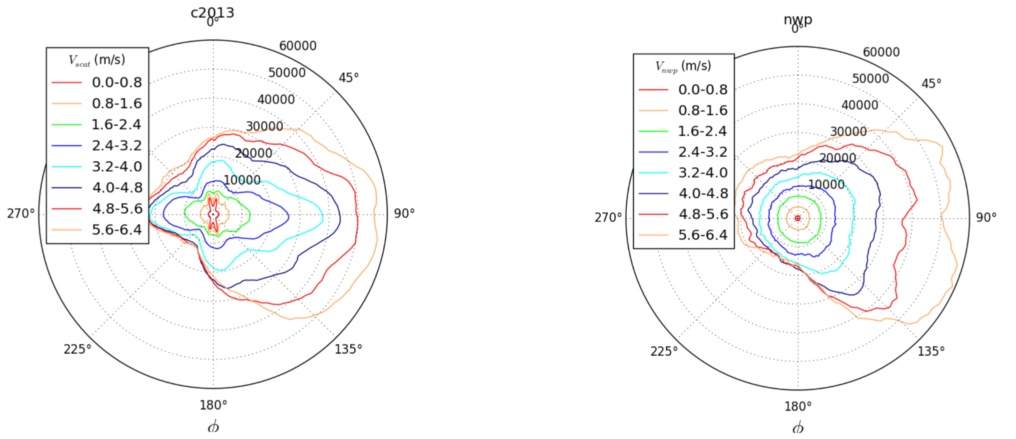

c) d)

Figure 16 – Wind direction distribution per wind speed interval for winds from a) CMOD6 and b) CMOD7. For reference c) C2013 and d) ECMWF are repeated.

In Figure 17 the wind speed distribution is shown for each WVC in the right swath for CMOD6, CMOD7, C2013 and NWP.

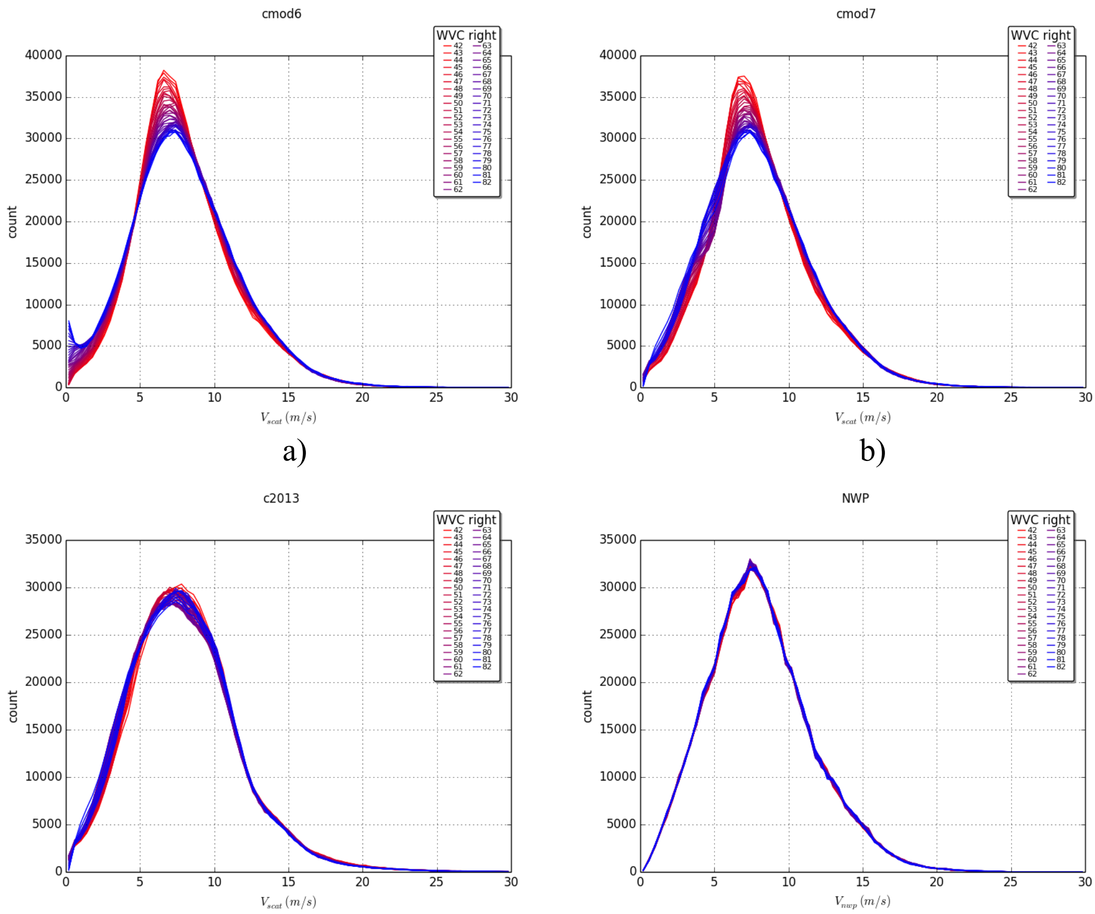

c) d)

Figure 17 – Wind speed distribution as function of WVC number for the right swath for winds from a) CMOD6 and b) CMOD7 c) C2013 and d) NWP.

For CMOD6 the most notable dependencies are those for low winds, where the high incidence angles give an unrealistic increase in the wind speed probability distribution function (pdf). The theoretical wind pdf that is based on Gaussian pdfs for the wind components u and v is a Weibull distribution that goes to zero linearly for small winds. Clearly, the dispersion of lines is much smaller at low winds for CMOD7 than for CMOD6. However, some dispersion remains in CMOD7 and C2013. Since the NWP winds do not show such dependency, it is likely that the dependency on WVC is artificial and caused by errors in the measurements, GMF or wind processing. Candidates that may cause WVC or incidence angle dependency are calibration, wind inversion, quality control and GMF model since they all depend on incidence angle.

For CMOD7 there still remains a dependency on incidence angle, where the pdf is narrowing for lower incidence angles.

C2013 shows the least WVC dependency in the pdfs and thus the best performance in this respect.

NWP shows only very small WVC dependency and all WVCs appear to sample very similar wind PDFs on a yearly basis.

In Figure 18 the Maximum Likelihood Estimate (MLE) is shown as a function of scatterometer wind speed for CMOD6 and CMOD7. For CMOD7 the asymmetry for winds around 5 m/s is less pronounced than for CMOD6 although it is not as symmetric as for C2013 (see Figure 9b). Due to the cone curvature it is not so clear how symmetric the MLE distribution should be after inversion. This may be further investigated by simulation.

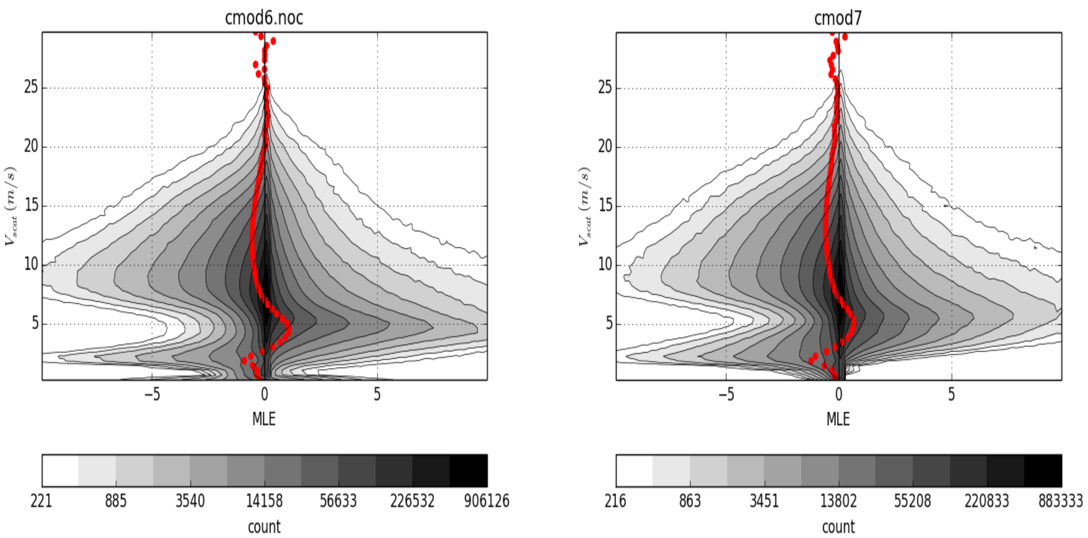

a) b)

Figure 18 – MLE as a function of scatterometer wind speed for a) CMOD6 and b) CMOD7.

In Figure 19 the averaged |MLE| and MLE are shown for CMOD6 and CMOD7 as a function of WVC number. The average values of the MLE are comparable for CMOD6 and CMOD7.

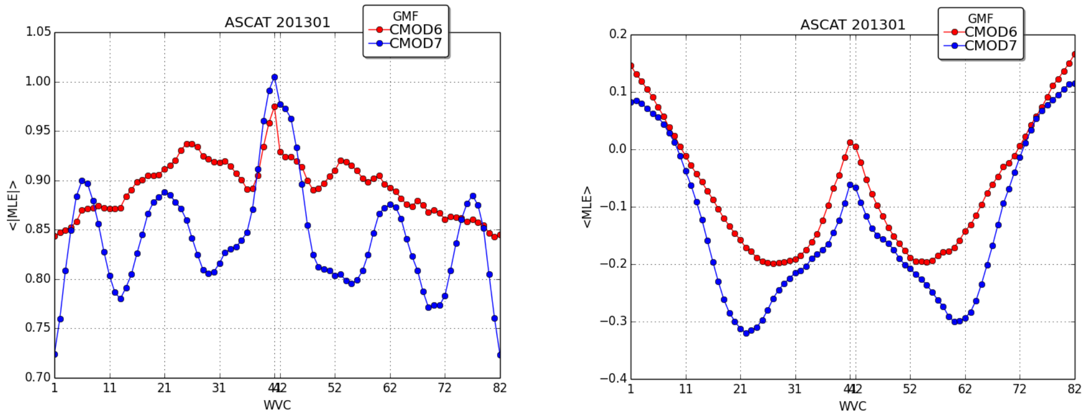

a) b)

Figure 19 – Average |MLE| and MLE as a function of WVC for CMOD6 and CMOD7.

In Figure 20 several QC flag rates are shown as a function of WVC number for CMOD6 and CMOD7. The top figures show overall flag rates and the bottom figures are for NWP winds lower than 6 m/s only.

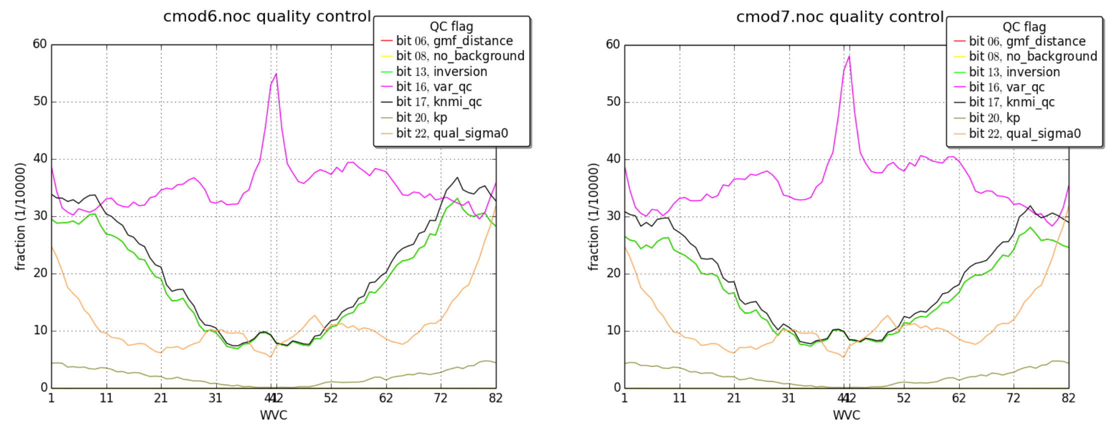

a) b)

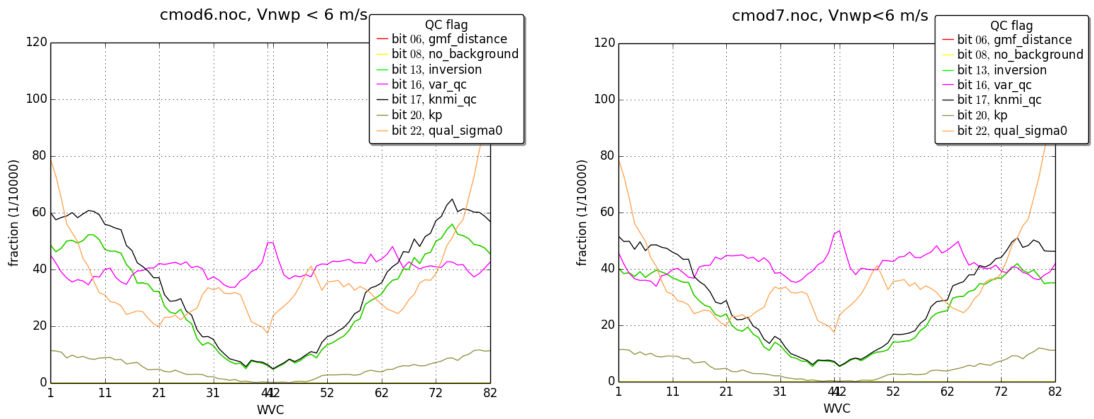

c) d)

Figure 20 – Quality Control rejection rate as a function of WVC number for CMOD6 and CMOD7. Figure c) and d) are for NWP winds lower than 6 m/s only.

As can be seen in the top figures the knmi_qc rejection rate is somewhat lower for CMOD7 compared to CMOD6, especially at high incidence angles. Identical normalization is used, and therefore we expect less rejection to be an improvement. The table below summarizes the rejection rates for CMOD6, CMOD7 and CMOD2013. As can be seen CMOD7 has the lowest total rejection rate. For low winds the rejection rate is lower than for CMOD6 so the gain is for the low winds as can be expected. The difference between C2013 and CMOD7 in inversion (KNMI_qc) and 2DVAR QC (var_qc) is intriguing and needs further investigation.

Table 2 - Quality Control rejections in 1000s

	total	knmi_qc	var_qc	rejections	rejection rate
cmod6	52646	110	185	295	0.0056
cmod7	52646	100	189	289	0.0055
c2013	52646	83	214	297	0.0056
cmod6 (Vnwp<6m/s)	16227	57	65	123	0.0076
cmod7 (Vnwp<6m/s)	16227	47	67	114	0.0070
c2013 (Vnwp<6m/s)	16227	36	70	106	0.0065

8 Buoy validation and triple collocations

In this section, scatterometer wind data are compared with in situ buoy wind measurements. The buoy winds are distributed through the Global Telecommunication System (GTS) and have been retrieved from the ECMWF MARS archive. The buoy data are quality controlled and (if necessary) blacklisted by ECMWF [Bidlot et al., 2002]. We used a set of approximately 150 moored non-coastal buoys spread over the oceans (most of them in the tropical oceans and near Europe and North America) which are also used in the buoy validations that are routinely performed for the OSI SAF wind products (see the links on http://www.knmi.nl/scatterometer/osisaf/). Most of these buoys are located more than 50 km off the coast.

See Figure 21 for the locations of the buoys used in the comparisons. A scatterometer wind and a buoy wind measurement are considered to be collocated if the distance between the WVC centre and the buoy location is less than the WVC spacing divided by √2 and if the acquisition time difference is less than 30 minutes.

The buoy winds are measured hourly by averaging the wind speed and direction over 10 minutes. The real winds at a given anemometer height have been converted to 10 m equivalent-neutral winds using the LKB model [Liu et al., 1979] in order to enable a good comparison with the 10 m scatterometer winds.

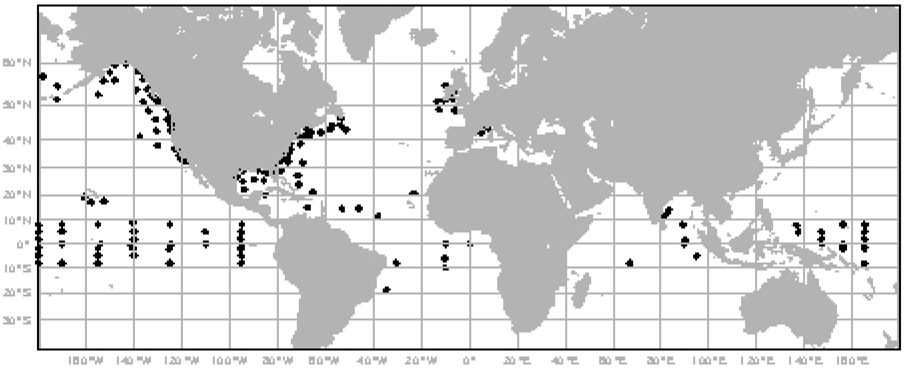

Figure 21 – Locations of the moored buoys used in the comparisons.

In Table 3 we compare the ASCAT buoy collocations for January 2013 for the three GMFs. CMOD7 gives the lowest standard deviation for the wind components. CMOD6 and C2013 have both higher standard deviations thus CMOD7 seems to have incorporated the best from both GMFs.

Table 3 – Buoy collocation results of ASCAT-B coastal wind products from January 2013 for the three GMFs.

ASCAT-B Coastal	# wind vectors	speed bias	stdev *u*	stdev *v*
CMOD6	2506	0.06	1.69	1.75
CMOD7	2506	0.13	1.65	1.73
C2013	2505	0.12	1.70	1.76

The detailed buoy collocation results in terms of wind speed, wind direction and wind components for the wind products are shown in
Figure 22.

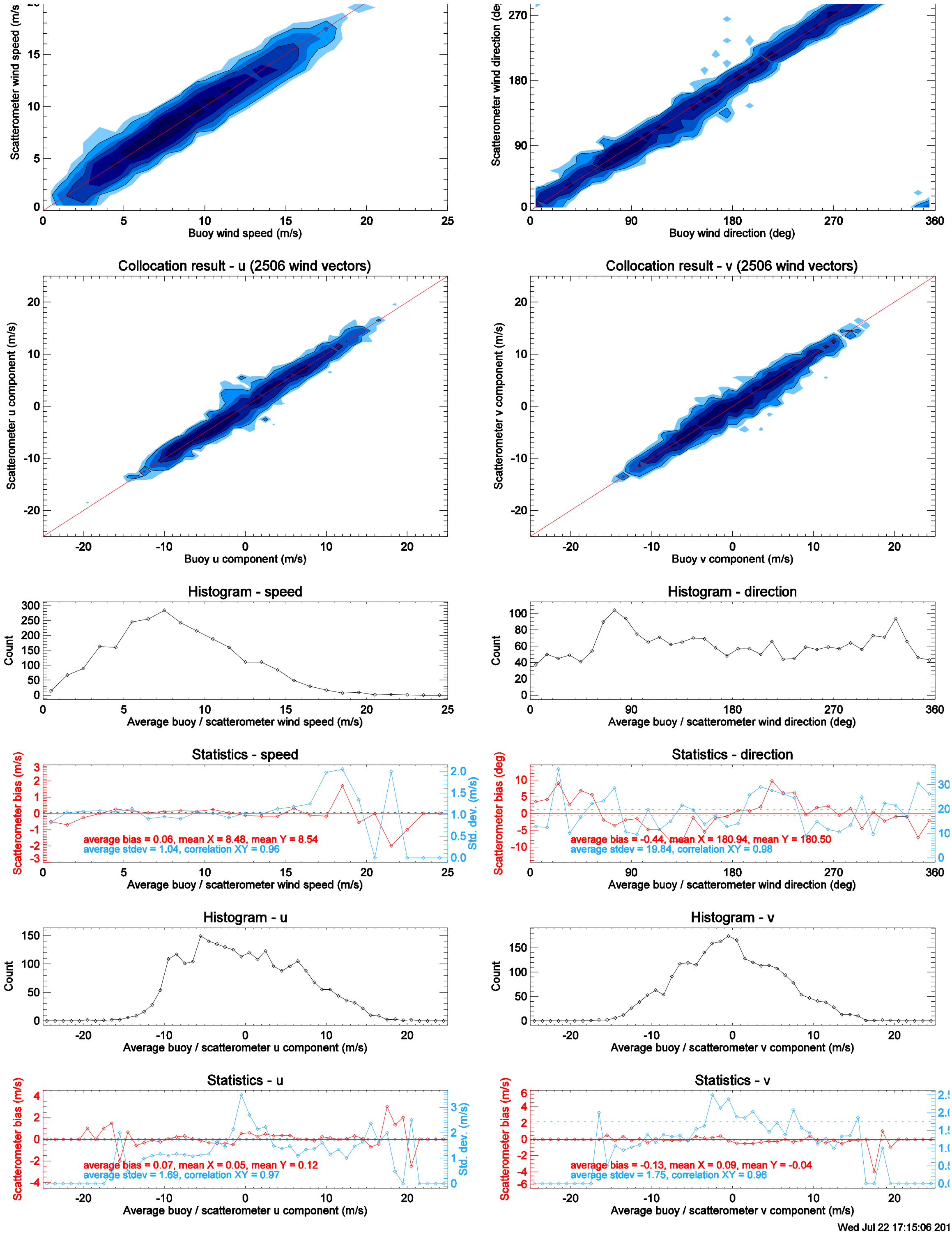

Scatterometer wind speed (m/s)
Buoy wind speed (m/s)
Scatterometer wind direction (deg)
Buoy wind direction (deg)
Collocation result - u (2506 wind vectors)
Scatterometer u component (m/s)
Buoy u component (m/s)
Collocation result - v (2506 wind vectors)
Scatterometer v component (m/s)
Buoy v component (m/s)
Histogram - speed
Count
Average buoy / scatterometer wind speed (m/s)
Histogram - direction
Count
Average buoy / scatterometer wind direction (deg)
Statistics - speed
Scatterometer bias (m/s)
Std. dev. (m/s)
average bias = 0.06, mean X = 8.48, mean Y = 8.54
average stdev = 1.04, correlation XY = 0.96
Average buoy / scatterometer wind speed (m/s)
Statistics - direction
Scatterometer bias (deg)
average bias = -0.44, mean X = 180.94, mean Y = 180.50
average stdev = 19.84, correlation XY = 0.98
Average buoy / scatterometer wind direction (deg)
Histogram - u
Count
Average buoy / scatterometer u component (m/s)
Histogram - v
Count
Average buoy / scatterometer v component (m/s)
Statistics - u
Scatterometer bias (m/s)
Std. dev. (m/s)
average bias = 0.07, mean X = 0.05, mean Y = 0.12
average stdev = 1.69, correlation XY = 0.97
Average buoy / scatterometer u component (m/s)
Statistics - v
Scatterometer bias (m/s)
average bias = -0.13, mean X = 0.09, mean Y = -0.04
average stdev = 1.75, correlation XY = 0.96
Average buoy / scatterometer v component (m/s)
Wed Jul 22 17:15:06 201

a) CMOD6

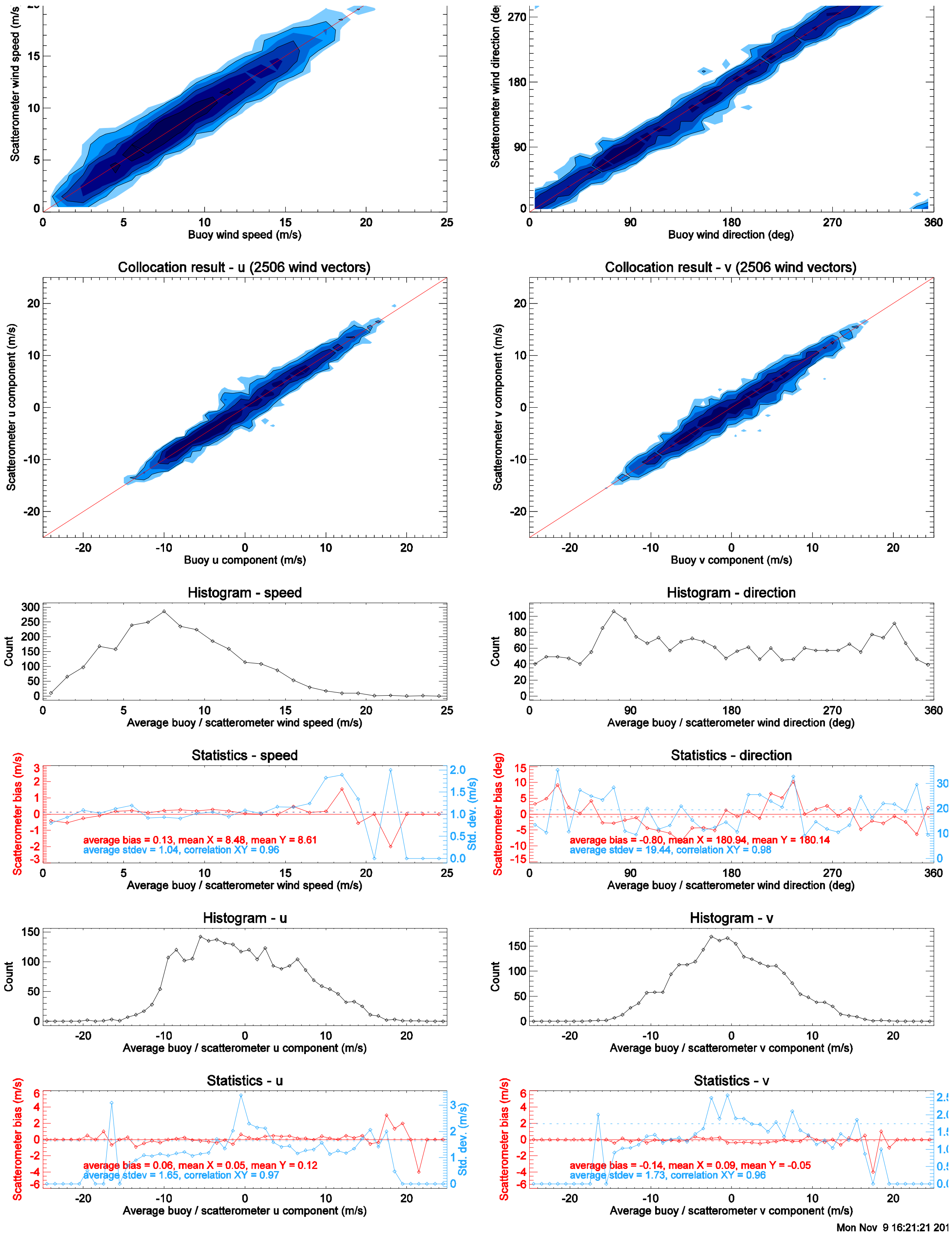

Scatterometer wind speed (m/s)
Buoy wind speed (m/s)
Scatterometer wind direction (de
Buoy wind direction (deg)
Collocation result - u (2506 wind vectors)
Scatterometer u component (m/s)
Buoy u component (m/s)
Collocation result - v (2506 wind vectors)
Scatterometer v component (m/s)
Buoy v component (m/s)
Histogram - speed
Count
Average buoy / scatterometer wind speed (m/s)
Histogram - direction
Count
Average buoy / scatterometer wind direction (deg)
Statistics - speed
Scatterometer bias (m/s)
Std. dev. (m/s)
average bias = 0.13, mean X = 8.48, mean Y = 8.61
average stdev = 1.04, correlation XY = 0.96
Average buoy / scatterometer wind speed (m/s)
Statistics - direction
Scatterometer bias (deg)
average bias = -0.80, mean X = 180.94, mean Y = 180.14
average stdev = 19.44, correlation XY = 0.98
Average buoy / scatterometer wind direction (deg)
Histogram - u
Count
Average buoy / scatterometer u component (m/s)
Histogram - v
Count
Average buoy / scatterometer v component (m/s)
Statistics - u
Scatterometer bias (m/s)
Std. dev. (m/s)
average bias = 0.06, mean X = 0.05, mean Y = 0.12
average stdev = 1.65, correlation XY = 0.97
Average buoy / scatterometer u component (m/s)
Statistics - v
Scatterometer bias (m/s)
average bias = -0.14, mean X = 0.09, mean Y = -0.05
average stdev = 1.73, correlation XY = 0.96
Average buoy / scatterometer v component (m/s)
Mon Nov 9 16:21:21 201

b) CMOD7

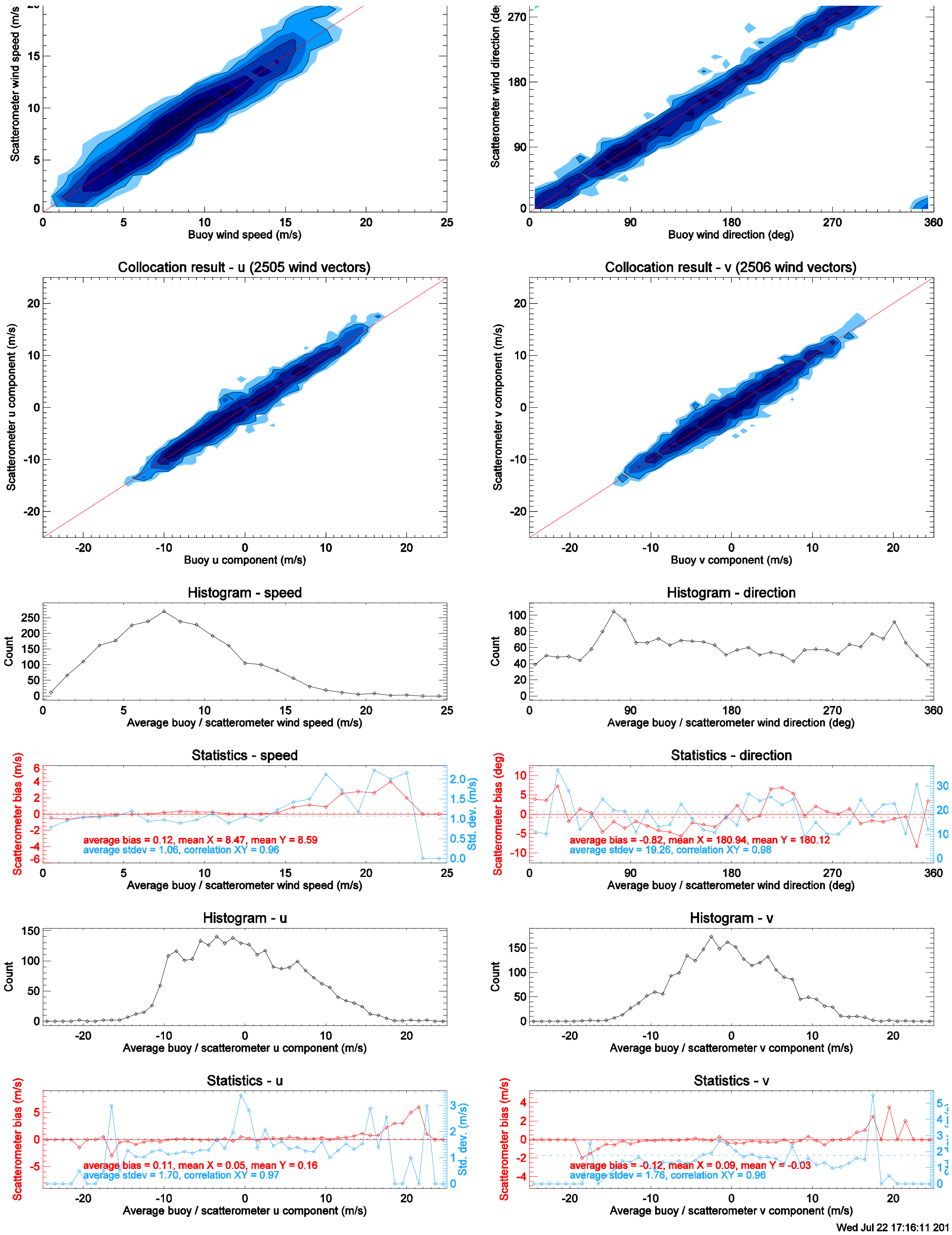

c) C2013

Figure 22 – Detailed scatterometer-buoy collocation results, showing biases of wind speed, direction (w.r.t. wind coming from the North), *u* and *v* components of ASCAT wind products versus the buoy winds from January 2013. The biases (red) and standard deviations (blue) as a function of the average scatterometer and model winds are shown. GMF a) CMOD6 b) CMOD7 and c) C2013 is used to generate the ASCAT winds.

A triple collocation study was performed to assess the errors of the ASCAT, ECMWF and buoy winds independently. The triple collocation method was introduced by [Stoffelen 1998]. Given a set of triplets of collocated measurements and assuming linear calibration, it is possible to simultaneously calculate the errors in the measurements and the relative calibration coefficients. The triple collocation method can give the measurement errors from the coarse resolution NWP model perspective or from the intermediate resolution scatterometer perspective and from the fine resolution buoy perspective with further assumptions on the local buoy measurement error. A sub WVC wind signal present in the buoy measurements, but not in the scatterometer winds is attributed as buoy error on the scatterometer scale (representativeness error). This matter is introduced in [Stoffelen 1998] and extensively discussed in [Vogelzang et al. 2011].

Collocated data sets of ASCAT coastal with ECMWF and buoy winds from January 2013 were used in the triple collocation. One month gives about 2500 collocations. Table 4 lists the error variances of the buoy, ASCAT and ECMWF winds from the intermediate resolution scatterometer perspective. The precision of the scatterometer error standard deviation is approximately 0.05 m/s, assuming that the error is Gaussian and that the representation error is known. For buoys, the precision estimate is 0.08 m/s and for ECMWF this is 0.06 m/s.

The errors in Table 4 are with respect to the scatterometer, so the representation error, calculated from the difference between scatterometer and ECMWF spectra, is added to the ECMWF background errors and subtracted from the buoy and scatterometer errors. Scatterometer errors for CMOD7 are lower than for CMOD6 and C2013.

Triple Collocation	Scatterometer		Buoys		ECMWF	
January 2013	σ_u (m/s)	σ_v (m/s)	σ_u (m/s)	σ_v (m/s)	σ_u (m/s)	σ_v (m/s)
CMOD6	0.77	0.88	1.20	1.26	1.55	1.54
CMOD7	0.69	0.83	1.20	1.25	1.56	1.54
C2013	0.76	0.87	1.20	1.26	1.53	1.54

Table 4 – Error standard deviations from triple collocation of ASCAT-B coastal wind products with buoy and ECMWF forecast winds, seen from the scatterometer perspective. The results were obtained for the month January 2013. ASCAT winds were produced with CMOD6, C2013 and CMOD7.

Glossary

AR - Ambiguity Removal
ASCAT - Advanced SCATterometer
AWDP - ASCAT Wind Data Processor
CMOD - C-band geophysical model function used for ERS and ASCAT
ESCAT - European Remote Sensing (ERS) SCATterometer
MLE - Maximum Likelihood Estimate
WVC - Wind Vector Cell

References

[Anderson et al, 2012] C. Anderson, J. Figa, H. Bonekamp, J. J. W. Wilson, J. Verspeek, A. Stoffelen, and M. Portabella, 2012: Validation of backscatter measurements from the advanced scatterometer on metop-a. J. Atmos. Oceanic Technol., 29, 77–88. doi: http://dx.doi.org/10.1175/JTECH-D-11-00020.1

[Bidlot et al, 2002] Bidlot J., D. Holmes, P. Wittmann, R. Lalbeharry, and H. Chen, Intercomparison of the performance of operational ocean wave forecasting systems with buoy data, Wea. Forecasting, vol. 17, 287-310, 2002

[Hersbach et al, 2007]
Hersbach, H., A. Stoffelen, and S. de Haan (2007), An improved C-band scatterometer ocean geophysical model function: CMOD5, J. Geophys. Res., 112, C03006, doi:10.1029/2006JC003743.

[Liu et al, 1979] Liu, W.T., K.B. Katsaros, and J.A. Businger, Bulk parameterization of air-sea exchanges of heat and water vapor including the molecular constraints in the interface, J. Atmos. Sci., vol. 36, 1979.

[Portabella and Stoffelen, 2006]
Marcos Portabella, Ad Stoffelen, Scatterometer backscatter uncertainty due to wind variability, IEEE Trans. Geosci. Rem. Sens. 44 (11), 3356-3362, 2006.

[Stoffelen and Anderson, 1997] Stoffelen, Ad, and David Anderson, "Scatterometer Data Interpretation: Measurement Space and inversion", J. Atm. and Ocean Techn., 14(6), 1298-1313, 1997.

[Ricciardulli, 2012], Lucrezia Ricciardulli and Frank Wentz, Development of Consistent Geophysical Model Functions for Different Scatterometer Missions: Ku and C, International Ocean Vector Wind Science Team Meeting, June 2012, Utrecht, the Netherlands
http://coaps.fsu.edu/scatterometry/meeting/docs/2012_meeting/New%20Products/Ricciardulli_IOVWST_2012_posted.pdf

[Ricciardulli, 2014], Lucrezia Ricciardulli and Frank Wentz, Progress and future plans on an ocean wind vector wind climate record. Products from OCEANSAT-2 Scatterometer, International Ocean Vector Wind Science Team Meeting, June 2014, Brest, France,
http://coaps.fsu.edu/scatterometry/meeting/docs/2014/ClimateDataRecord/Ricciardulli_ovwst_2014_CDR_posted.pdf

[Stoffelen, 1998] Stoffelen, A., Toward the true near-surface wind speed: error modelling and calibration using triple collocation, J. Geophys. Res. 103C4, 7755-7766, 1998.

[Scirocco team, 2014] Scirocco scatterometry handbook, SCI-SPU-14-0001-v01, 20-08-2014

[Verspeek, 2012], J. Verspeek et al (2012) "Improved ASCAT Wind Retrieval Using NWP Ocean Calibration", IEEE Transactions on Geoscience and Remote Sensing, vol 50, pp 2488 - 2494, doi: 10.1109/TGRS.2011.2180730.

[Vogelzang et al, 2011] Vogelzang, J., A. Stoffelen, A. Verhoef, and J. Figa-Saldaña (2011), On the quality of high-resolution scatterometer winds, J. Geophys. Res., 116, C10033, doi:10.1029/2010JC006640.